J. Appl. Comput. Mech., xx(x) (2026) 1-15
DOI: 10.22055/jacm.2026.49578.6088

ISSN: 2383-4536
jacm.scu.ac.ir

Shahid Chamran University of Ahvaz

Journal of
Applied and Computational Mechanics

Research Paper

# A Nonlinear Integral Equation for Finite-Deflection Analysis of an Euler–Bernoulli Beam with Variable Bending Stiffness

**Mirosław Sadowski**

Independent Researcher, Zgorzelec, Poland, Email: miroslaw.sadowski@gmail.com

Received July 16 2026; Revised August 20 2026; Accepted for publication September 02 2026.
✉ Corresponding author: M. Sadowski (miroslaw.sadowski@gmail.com)


**Abstract.** This paper derives an equivalent nonlinear Volterra integral equation with Hammerstein-type nonlinearity for the analysis of a planar, inextensible Euler–Bernoulli beam with variable bending stiffness subjected to a conservative compressive dead load. The proposed integral equation is obtained by transforming the governing nonlinear differential equation into an equivalent integral form. Selected properties of the resulting nonlinear operator are analysed, and the formulation is shown to be consistent with the classical Euler buckling theory in the limit of small rotations. The proposed equation is solved numerically using the Nyström method and illustrated by a beam with locally degraded bending stiffness. The numerical example determines the compressive load corresponding to a prescribed finite-deflection equilibrium configuration. The results demonstrate that the proposed integral formulation provides a convenient framework for the analytical and numerical investigation of geometrically nonlinear equilibrium problems involving Euler–Bernoulli beams with variable bending stiffness.

**Keywords:** Buckling, geometric nonlinearity, integral equations, Volterra–Hammerstein equation, nonlinear operator, variable bending stiffness.

## 1. Introduction

The stability of slender structural members has long been one of the oldest and, at the same time, one of the most fundamental topics in structural mechanics [1]. Buckling under compressive loading often determines the load-carrying capacity of a structure, occurring at stress levels significantly below the material strength limit [2]. For this reason, the accurate determination of the critical load and its corresponding buckling mode has remained a major research topic in beam and column stability theory for more than two centuries. The results of these studies are widely applied in the design of columns, masts, trusses, bridge components, aerospace structures, mechanical systems, and many other engineering applications in which structural stability constitutes the governing design criterion [3, 4].

The origins of modern stability theory are generally attributed to the pioneering work of Leonhard Euler [5], who first determined the critical load of an ideal compressed column. Euler demonstrated that buckling can be formulated as an equilibrium problem of the deformed beam axis and is obtained by solving an appropriate differential equation together with the corresponding boundary conditions. His work became one of the milestones of structural mechanics and initiated the systematic development of mathematical models describing the behaviour of beam-like structures. Since then, stability theory has evolved alongside elasticity theory and continuum mechanics, giving rise to increasingly sophisticated models of structural behaviour [6]. Over the years, the classical buckling equation has been systematically extended to account for various support conditions, different loading configurations, shear deformation, geometric imperfections, residual stresses, and interactions with elastic foundations [7]. At the same time, models describing beams with variable cross-sections and spatially non-uniform material properties have also been developed [8]. The nonlinear stability of beams with variable cross-sections or spatially varying bending stiffness has also attracted considerable attention. Analytical and numerical studies have addressed large-deflection elastica problems for variable-cross-section beams, the buckling of columns with continuously varying flexural rigidity, and the analysis of elastic curves with spatially varying bending stiffness, demonstrating the strong influence of stiffness distribution on the equilibrium configuration and critical load of non-uniform structural members [9-11]. Despite their diversity, these models share a common feature: their mathematical formulation is based on a differential equation derived from equilibrium conditions together with the constitutive relationship between the bending moment and the curvature of the beam axis [12]. One of the most widely used formulations is the Euler–Bernoulli beam equation, which for a beam with variable bending stiffness is written as:

$$(EI(x)w''(x))'' + Fw''(x) = 0 \tag{1}$$

Published online: September 04 2026

where $EI(x)$ denotes the bending stiffness, $F$ is the compressive force, and $w(x)$ represents the transverse displacement of the beam axis [13]. Although linear, this equation serves as the starting point for numerous models employed in both linear buckling analysis and a wide range of optimization and parameter identification problems. For homogeneous beams it admits many well-known analytical solutions [14]; however, even a slight generalization of the model substantially increases its mathematical complexity. An additional source of difficulty arises from geometric nonlinearity. For large deflections, the classical relationship between the transverse displacement and the beam curvature is no longer sufficient, and the governing equilibrium equations become nonlinear differential equations with variable coefficients [15]. The geometrically nonlinear behaviour of slender beams has been investigated using a variety of elastica formulations differing in their kinematic assumptions and mathematical complexity. Kinematically exact beam theories have considerably extended the classical elastica framework, enabling an accurate description of finite rotations and large displacements. Both extensible and inextensible Euler–Bernoulli beam formulations have been developed for the analysis of geometrically nonlinear beam behaviour. In particular, extensible elastica formulations based on kinematically exact beam theory have been used to investigate the influence of axial extensibility on buckling behaviour [16]. The applicability of geometrically exact and second-order beam theories to buckling and post-buckling analysis has also been systematically investigated [17]. More recently, geometrically exact nonlinear beam models for large deformation analysis [18] and geometrically exact Euler–Bernoulli beam elements for nonlinear structural analysis [19] have further expanded the available modelling approaches. Simultaneously accounting for spatially varying bending stiffness and an exact geometric description of the deformed beam leads to models whose analytical solution is available only in a limited number of special cases. Consequently, numerical techniques remain the dominant approach, including the finite element method, spectral methods, the Galerkin and Rayleigh–Ritz procedures, and various iterative algorithms [20].

Despite their high computational efficiency, these numerical approaches operate directly on the governing differential equation or its discrete representation. As a consequence, they primarily focus on obtaining the solution itself, while providing relatively limited insight into the properties of the underlying operator. Integral-equation formulations have also been employed in the analysis of beam buckling and related stability problems, providing an alternative representation of the governing boundary-value problem while preserving its mechanical equivalence [21]. From a mathematical perspective, such formulations also enable the use of tools from functional analysis and nonlinear operator theory [22]. The transformation into an integral form is therefore not merely a formal mathematical manipulation but provides a fundamentally different representation of the governing operator, potentially facilitating both theoretical investigations and the development of efficient numerical methods. In many areas of applied mathematics, integral equations constitute the basis for studying the existence and uniqueness of solutions, their qualitative properties, and the construction of effective approximation techniques [23,24]. In particular, the analytical theory of nonlinear Volterra–Hammerstein equations and the corresponding numerical methods, including quadrature- and collocation-based approaches, have been extensively developed [25].

Despite the extensive use of integral equations in continuum mechanics and mathematical physics, their application to geometrically nonlinear beams with variable bending stiffness have received relatively little attention. Existing studies are mainly devoted to the direct solution of nonlinear differential equations, whereas the transformation of such equations into equivalent integral formulations has not yet been investigated in depth. To the best of the author's knowledge, no angle-based nonlinear Volterra–Hammerstein integral formulation has been reported for the planar inextensible Euler–Bernoulli beam with spatially variable bending stiffness. This is particularly true for models that simultaneously account for spatially varying bending stiffness and an exact geometric description of the deformed beam axis.

The objective of the present work is to derive an equivalent nonlinear Volterra–Hammerstein integral equation corresponding to the geometrically nonlinear model of the Euler–Bernoulli beam with variable bending stiffness. The analysis starts from the governing equilibrium equation in differential form, which is subsequently transformed into an equivalent integral formulation. The resulting equation remains fully consistent with the original mechanical model while providing a convenient framework for further operator-theoretic analysis and for the development of new solution techniques for nonlinear buckling problems. The proposed formulation provides a rigorous operator-based representation of the governing nonlinear problem and may serve as a foundation for further analytical and numerical studies of geometrically nonlinear stability problems involving structural members with non-uniform mechanical properties.

The remainder of the paper is organized as follows. Section 2 introduces the geometrically nonlinear beam model and its mechanical assumptions. Section 3 derives the equivalent nonlinear integral formulation. Section 4 discusses selected analytical properties of the resulting nonlinear operator. Section 5 presents the numerical solution, convergence and verification studies, and a parametric analysis of the variable-stiffness beam. Finally, Section 6 summarizes the main conclusions and outlines directions for further research.

## 2. Geometrically Nonlinear Model of a Beam with Variable Bending Stiffness

Consider a slender Euler–Bernoulli beam [26] of length $L$, subjected to an axial compressive force $F$. The beam is supported by a pin at the left end and by an axially movable roller at the right end, as shown in Fig. 1. Throughout this paper, the term *beam* is used in accordance with the terminology of the Euler–Bernoulli beam theory and refers to the slender structural member considered in the present stability analysis.

The beam is modelled as an initially straight, planar and inextensible Euler–Bernoulli elastica. The beam material is assumed to be linearly elastic and to obey Hooke's law [27]. Shear deformation is neglected, while the cross-sections remain plane and perpendicular to the deformed centreline [28]. No restriction is imposed on the magnitude of the transverse displacement or the cross-sectional rotation, allowing the model to account for full geometric nonlinearity. The right support permits axial translation during deformation while preventing transverse displacement, which is consistent with the adopted inextensible elastica formulation.

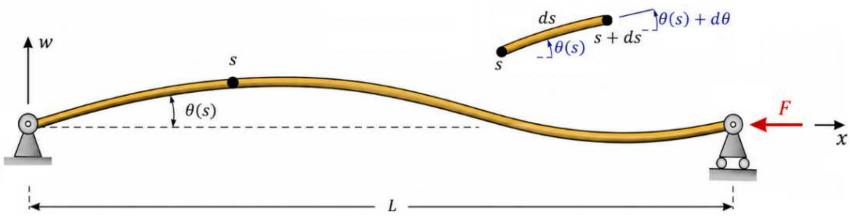


**Fig. 1.** Structural model of the beam.

Let $s$ denotes the material arc-length coordinate of the initially straight beam centreline:

$$s \in [0, L], \tag{2}$$

Here, $L$ denotes the undeformed material length of the beam. Owing to the inextensibility assumption, it is also equal to the arc length of the deformed centreline. The same material coordinate $s$ therefore parameterizes the deformed configuration, whose position vector is written as:

$$\mathbf{r}(s) = (x(s), w(s)). \tag{3}$$

The tangent vector to the deformed centreline is defined by:

$$\mathbf{t}(s) = \mathbf{r}'(s) \tag{4}$$

where the prime denotes differentiation with respect to $s$. The inextensibility condition requires:

$$\|\mathbf{r}'(s)\| = 1. \tag{5}$$

Let $\theta(s)$ denotes the angle between the tangent to the deformed centreline and the undeformed beam axis. The unit tangent vector may then be expressed as [29]

$$\mathbf{t}(s) = (\cos\theta(s), \sin\theta(s)). \tag{6}$$

Consequently, the coordinates of the deformed centreline satisfy:

$$x'(s) = \cos\theta(s), \quad w'(s) = \sin\theta(s). \tag{7}$$

The corresponding unit normal vector is:

$$\mathbf{n}(s) = (-\sin\theta(s), \cos\theta(s)). \tag{8}$$

The curvature of the deformed centreline is therefore given by [30]:

$$\kappa(s) = \mathbf{t}'(s) \cdot \mathbf{n}(s) = \theta'(s). \tag{9}$$

The bending stiffness is prescribed as a positive function of the material coordinate:

$$EI = EI(s), \quad EI(s) > 0. \tag{10}$$

The bending moment is related to the curvature through the linear elastic constitutive relation [31]:

$$M(s) = EI(s)\,\kappa(s) \tag{11}$$

and hence,

$$M(s) = EI(s)\,\theta'(s). \tag{12}$$

For a conservative compressive dead load acting along the undeformed beam axis, the internal force vector is constant and may be written as:

$$\mathbf{N} = (-F, 0). \tag{13}$$

The local equilibrium of moments acting on an infinitesimal beam element, together with Eqs. (6), (12), and (13), yields the geometrically nonlinear equilibrium equation of a beam with variable bending stiffness [11]:

$$\left(EI(s)\,\theta'(s)\right)' + F\sin\theta(s) = 0. \tag{14}$$

To replace the trigonometric nonlinearity with an algebraic one, the substitution:

$$u(s) = \sin\frac{\theta(s)}{2}. \tag{15}$$

is introduced. The corresponding trigonometric identities yield:

$$\sin\theta(s) = 2u(s)\sqrt{1 - u^2(s)}, \tag{16}$$

and,

$$\theta(s) = 2\arcsin u(s), \tag{17}$$

which gives:

$$\theta'(s) = \frac{2u'(s)}{\sqrt{1 - u^2(s)}}. \tag{18}$$

Substituting Eqs. (16) and (18) into Eq. (14) leads to:

$$\left(EI(s)\frac{u'(s)}{\sqrt{1 - u^2(s)}}\right)' + Fu(s)\sqrt{1 - u^2(s)} = 0. \tag{19}$$

Expanding the derivative and rearranging the resulting expression yields the equivalent nonlinear differential equation:

$$u''(s)+\frac{\left(EI(s)\right)'}{EI(s)}u'(s)+\frac{u(s)}{1-u^2(s)}\left(u'(s)\right)^2+\frac{F}{EI(s)}\left(1-u^2(s)\right)u(s)=0. \tag{20}$$

Although the subsequent integral formulation is derived directly in terms of the rotation angle $\theta(s)$, Eq. (20) is retained as an equivalent algebraic representation of the governing nonlinear differential equation. The inverse relation $\theta(s)=2\arcsin(u(s))$ is understood on the principal branch, corresponding to $|\theta(s)|<\pi$ and hence $|u(s)|<1$. Within this range, the transformation is one-to-one and the denominators appearing in Eqs. (18)–(20) remain non-zero. The transformed equation eliminates the trigonometric nonlinearity and may be useful for subsequent analytical investigations and numerical solution methods.

For the beam considered here, the mechanical boundary conditions require the bending moments to vanish at both ends:

$$M(0)=0,\quad M(L)=0. \tag{21}$$

Using Eq. (12) and taking into account that the bending stiffness is positive at both beam ends, these conditions are equivalent to:

$$\theta'(0)=0,\quad \theta'(L)=0. \tag{22}$$

These conditions express the absence of bending moments at the pin and roller supports. Furthermore, because both supports remain at the same transverse level, Eq. (7) yields the geometric compatibility condition:

$$w(L)-w(0)=\int_0^L \sin\theta(s)ds=0. \tag{23}$$

No additional condition involving $\int_0^L \cos\theta(s)ds$ is imposed, because the roller support permits axial translation and the horizontal separation of the supports is therefore not prescribed during deformation. From Eq. (18), the moment boundary conditions for the transformed variable become:

$$u'(0)=0,\quad u'(L)=0. \tag{24}$$

## 3. Transformation into an Equivalent Nonlinear Integral Equation

Equation (20) provides a convenient algebraic representation of the geometrically nonlinear model. However, the presence of nonlinear terms involving derivatives of the unknown function makes its direct transformation into an integral form difficult. Therefore, Eq. (14) is adopted as the governing equation in the subsequent analysis, since its structure allows an exact transformation into an equivalent nonlinear integral equation. The resulting formulation remains fully consistent with the original mechanical model and provides the basis for further analysis.

Integrating Eq. (14) yields:

$$EI(s)\theta'(s)-EI(0)\theta'(0)=-F\int_0^s \sin\theta(\xi)d\xi. \tag{25}$$

From the boundary condition (23), $\theta'(0)=0$, and therefore Eq. (25) becomes:

$$EI(s)\theta'(s)=-F\int_0^s \sin\theta(\xi)d\xi. \tag{26}$$

In the following, $EI(s)$ is assumed to be continuous and positive over the interval under consideration, i.e., $EI(s)\in C_{[0,L]}$ and $EI(s)>0$. This assumption ensures that the integral kernel is well defined and excludes possible singularities of the operator. Hence, Eq. (26) may be written as:

$$\theta'(s)=-\frac{F}{EI(s)}\int_0^s \sin\theta(\xi)d\xi. \tag{27}$$

Equation (27) is an intermediate integro-differential form of the problem. The derivative of the unknown function at the point $s$is expressed in terms of an integral involving the values of $\theta$, whereas the effect of the variable bending stiffness appears through the factor $1/EI(s)$. Integrating once more gives:

$$\int_0^s \theta'(\eta)d\eta=-F\int_0^s \frac{1}{EI(\eta)}\left(\int_0^\eta \sin\theta(\xi)d\xi\right)d\eta \tag{28}$$

and therefore,

$$\theta(s)=\theta(0)-F\int_0^s \frac{1}{EI(\eta)}\left(\int_0^\eta \sin\theta(\xi)d\xi\right)d\eta. \tag{29}$$

Equation (29) contains a double integral defined over the region:

$$D_s=\left\{(\xi,\eta):0\le\xi\le\eta\le s\right\}, \tag{30}$$

which, for a fixed value of $s$, may equivalently be described by:

$$0\le\xi\le s,\quad \xi\le\eta\le s \tag{31}$$

Changing the order of integration therefore gives:

$$\int_0^s \frac{1}{EI(\eta)}\left(\int_0^\eta \sin\theta(\xi)\,d\xi\right)d\eta = \int_0^s\left(\int_\xi^s \frac{d\eta}{EI(\eta)}\right)\sin\theta(\xi)\,d\xi. \tag{32}$$

Substituting Eq. (32) into Eq. (29) yields:

$$\theta(s) = \theta(0) - F\int_0^s\left(\int_\xi^s \frac{d\eta}{EI(\eta)}\right)\sin\theta(\xi)\,d\xi. \tag{33}$$

To simplify the notation and isolate the influence of the variable bending-stiffness distribution, the function:

$$K(s,\xi) = \int_\xi^s \frac{d\eta}{EI(\eta)}, \tag{34}$$

is introduced, where $0 \le \xi \le s \le L$. The function $K(s,\xi)$ serves as the integral kernel and contains complete information about the bending-stiffness distribution along the beam. For a prescribed function $EI(s)$, the kernel is known, while its form depends directly on the spatial variation of the mechanical properties of the member. It also follows from its definition that $K(s,s)=0$, whereas for $s > \xi$, the function $K(s,\xi)$ is positive and non-decreasing with respect to $s$.

Using the notation introduced in Eq. (34), Eq. (33) can be written in the compact form:

$$\theta(s) = \theta(0) - F\int_0^s K(s,\xi)\sin\theta(\xi)\,d\xi. \tag{35}$$

For a prescribed initial rotation $a = \theta(0)$, Eq. (35) is a nonlinear Volterra integral equation of the second kind with a Hammerstein-type nonlinearity. Its Volterra character results from the variable upper integration limit $s$, whereas its Hammerstein-type nonlinearity follows from the separation of the linear integral operator, defined by the kernel $K(s,\xi)$, from the nonlinear function $\sin\theta(\xi)$, which depends on the solution [32, 33].

In general form, the nonlinear Volterra integral equation with Hammerstein-type nonlinearity may be written as:

$$\theta(s) = f(s) - F\int_0^s K(s,\xi)\sin\theta(\xi)\,d\xi \tag{36}$$

where, for the problem considered here:

$$f(s) = a, \tag{37}$$

and,

$$g(\xi,\theta(\xi)) = -F\sin\theta(\xi). \tag{38}$$

Thus, the nonlinearity of the model is contained entirely in the function $g$, whereas the influence of the variable bending stiffness is fully incorporated into the kernel $K(s,\xi)$. The resulting nonlinear integral equation contains no derivatives of the unknown function, which distinguishes it from the original differential formulation and facilitates further operator-theoretic analysis. For a prescribed value $a = \theta(0)$, Eq. (35) defines a nonlinear Volterra integral equation for the rotation field $\theta(0)$. The left-end moment condition $\theta'(0)=0$ is already incorporated into this equation through the first integration of the governing differential equation. Thus, for prescribed $a$ and $F$, Eq. (35) has the character of an initial-value Volterra problem. To recover the original two-point boundary-value problem, the right-end moment condition $\theta'(L)=0$ must additionally be satisfied. Substituting $s = L$ into Eq. (27) gives:

$$\theta'(L) = -\frac{F}{EI(L)}\int_0^L \sin\theta(\xi)\,d\xi. \tag{39}$$

For $F \ne 0$ and $EI(L) > 0$, satisfaction of the condition $\theta'(L)=0$ requires:

$$\int_0^L \sin\theta(\xi)\,d\xi = 0. \tag{40}$$

Equation (40) is the scalar compatibility condition corresponding to the right-end moment condition $\theta'(L)=0$. For a prescribed value $a=\theta(0)$, this condition selects the admissible value of the compressive load $F$ for which the solution of the Volterra equation also satisfies the second endpoint moment condition. Consequently, the complete nonlinear problem is not represented by the Volterra equation alone, but by an augmented system for the unknown pair $(\theta, F)$. The geometrically nonlinear equilibrium problem may therefore be written as:

$$\begin{array}{ll}\theta(s) = a - F\displaystyle\int_0^s K(s,\xi)\sin\theta(\xi)\,d\xi, & \\ & a(0)\text{ prescribed.} \\ \displaystyle\int_0^L \sin\theta(\xi)\,d\xi, & \end{array} \tag{41}$$

Hence, for each prescribed finite rotation amplitude $a$, system (41) determines simultaneously the corresponding equilibrium rotation field $\theta(s)$ and the admissible compressive load $F$. The equivalence of the two formulations can also be demonstrated in the reverse direction. Differentiating the first equation in Eq. (41) with respect to $s$ and using:

$$\frac{\partial K(s,\xi)}{\partial s} = \frac{1}{EI(s)} \tag{42}$$

one obtains:

$$\theta'(s) = -\frac{F}{EI(s)}\int_0^s \sin\theta(\xi)\,d\xi, \tag{43}$$

which is identical to Eq. (27). This relation, in turn, leads back to Eq. (14).

The resulting formulation separates the contributions of the individual components of the model. The variation of the bending stiffness is represented by the kernel $K(s,\xi)$, the compressive load appears as the parameter $F$, and the geometric nonlinearity is described by the function $\sin\theta$. This structure makes it possible to treat the problem as a fixed-point problem for an appropriate nonlinear operator and provides the basis for a further investigation of the properties of its solutions.

## 4. Properties of the Nonlinear Integral Operator

For a prescribed initial rotation $a = \theta(0)$, define the affine subset:

$$X_a = \{\theta \in C([0,L];\mathbb{R}) : \theta(0) = a\} \tag{44}$$

where $C([0,L];\mathbb{R})$ is equipped with the supremum norm $\|\theta\|_\infty = \max_{s\in[0,L]}|\theta(s)|$. The analysis is carried out for prescribed $a \in \mathbb{R}$ and $F > 0$. As assumed in Section 3, $EI \in C([0,L])$ and $EI(s) > 0$ for all $s \in [0,L]$. Under these assumptions, the kernel $K(s,\xi)$ defined by Eq. (34) is continuous on the triangular domain $0 \le \xi \le s \le L$. For fixed $a$ and $F$, define the nonlinear operator $T_{a,F} : X_a \to X_a$ by:

$$(T_{a,F}\theta)(s) = a - F\int_0^s K(s,\xi)\sin\theta(\xi)\,d\xi. \tag{45}$$

Since the integral vanishes at $s = 0$, one has $(T_{a,F}\theta)(0) = a$ and hence $T_{a,F}\theta \in X_a$. Therefore, the operator is well defined on $X_a$. The right-end moment condition is represented separately by the scalar compatibility functional $C(\theta) = \int_0^L \sin\theta(\xi)d\xi$. Accordingly, for a prescribed amplitude $a$, the complete nonlinear equilibrium problem consists in finding the pair $(\theta,F)$ such that $\theta = T_{a,F}\theta$, $C(\theta) = 0$. The fixed-point equation $\theta = T_{a,F}\theta$ represents the nonlinear Volterra integral equation for prescribed $a$ and $F$, whereas the scalar compatibility condition $C(\theta) = 0$ enforces the right-end moment condition and selects the admissible value of the compressive load $F$.

### 4.1. Influence of the bending-stiffness distribution on the integral kernel

The kernel of the operator $T_{a,F}$ is defined by Eq. (34). This relation shows that all information concerning the bending-stiffness distribution is contained in the function $K(s,\xi)$. Consequently, a change in $EI(s)$ does not affect the form of the geometric nonlinearity, but only modifies the kernel of the operator. Consider two bending-stiffness distributions $EI_1(s)$ and $EI_2(s)$ such that $EI_1(s) \le EI_2(s)$ for all $s \in [0,L]$, and let $K_1(s,\xi)$ and $K_2(s,\xi)$ denote the corresponding kernels. It follows directly from Eq. (34) that $K_1(s,\xi) \ge K_2(s,\xi)$ for $0 \le \xi \le s \le L$. Thus, a pointwise reduction in bending stiffness leads to a pointwise increase in the corresponding integral kernel. For fixed $a$, $F$ and $\theta$, this ordering determines the corresponding change in the kernel contribution to the nonlinear integral operator.

From a mathematical point of view, the operator $T_{a,F}$ retains the same functional form regardless of the particular distribution of $EI(s)$; only the kernel $K(s,\xi)$ changes. This makes it possible to represent both homogeneous beams and beams with spatially variable bending stiffness within the same operator framework. Since $EI \in C([0,L])$ and $EI(s) > 0$ for all $s \in [0,L]$, there exists a positive minimum bending stiffness $EI_{\min} = \min_{s\in[0,L]} EI(s) > 0$. Therefore, from the definition of the kernel in Eq. (34), for $0 \le \xi \le s \le L$, $0 \le \int_\xi^s d\eta / EI(\eta) \le (s-\xi)/EI_{\min} \le L/EI_{\min}$. Thus, the kernel is uniformly bounded on the triangular domain $0 \le \xi \le s \le L$, with $\|K\|_\infty \le L/EI_{\min}$. This estimate provides a direct quantitative relation between the minimum bending stiffness and the magnitude of the integral kernel and will be used below in the analysis of the nonlinear operator.

It should be emphasized, however, that the pointwise ordering of the kernels does not by itself imply a corresponding monotonic ordering of the finite-amplitude equilibrium loads. In the nonlinear problem, the rotation field $\theta$ entering the function $\sin\theta$ also depends on the bending-stiffness distribution and is determined simultaneously with the admissible load $F$. Therefore, the kernel ordering established above should be distinguished from any monotonicity property of the nonlinear equilibrium load.

### 4.2. Influence of the compressive load

The compressive load $F$ enters the operator $T_{a,F}$ in Eq. (45) as a parameter multiplying the integral term. For fixed $a$, $EI(s)$ and $\theta$, an increase in $F$ therefore increases the magnitude of the integral contribution without changing the functional form of the operator.

In the complete equilibrium problem, however, $F$ is not prescribed independently. For a given amplitude $a$, its admissible value is determined together with the rotation field $\theta(s)$ by the fixed-point equation and the scalar compatibility condition. Thus, $F$ acts both as a parameter of the nonlinear Volterra operator and as an unknown load level selected by the right-end moment condition.

### 4.3. Nature of the operator nonlinearity

The operator $T_{a,F}$ defined by Eq. (45) is nonlinear with respect to $\theta$ solely because of the function $\sin\theta$. Indeed, for two functions $\theta_1$ and $\theta_2$ arbitrary real constants $\alpha$ and $\beta$ :

$$\sin(\alpha\theta_1 + \beta\theta_2) \ne \alpha\sin\theta_1 + \beta\sin\theta_2, \tag{46}$$

in general. Therefore, the dependence of the operator on the rotation field does not satisfy the principle of superposition. The nonlinearity of the model is purely geometric and does not arise from the constitutive relation, which remains linear.

It should also be emphasized that derivatives of the unknown function do not appear under the integral sign. In comparison with the differential equation (14), this provides a simpler operator representation while preserving the full geometric nonlinearity of the adopted elastica model.

### 4.4. Linear limit

For small values of the rotation angle, i.e.,

$$|\theta(s)| \ll 1, \tag{47}$$

the classical approximation:

$$\sin\theta(s) \approx \theta(s) \tag{48}$$

may be adopted. Equation (35) then reduces to:

$$\theta(s) = a - F\int_0^s K(s,\xi)\theta(\xi)\,d\xi. \tag{49}$$

where $a = \theta(0)$ is prescribed. Equation (49), together with the linearized compatibility condition:

$$\int_0^L \theta(\xi)\,d\xi = 0, \tag{50}$$

represents the small-rotation limit of the nonlinear formulation. To identify the bifurcation load, the linearization is considered about the trivial equilibrium state $\theta \equiv 0$, corresponding to $a \equiv 0$. The resulting homogeneous linearized problem is

$$\theta(s) = -F\int_0^s K(s,\xi)\theta(\xi)\,d\xi, \tag{51}$$

supplemented by the compatibility condition (50). Non-trivial solutions of Eqs. (50) and (51) exist only for discrete values of $F$, which constitute the eigenvalues of the linearized stability problem. The equivalence with the corresponding differential eigenvalue problem follows directly by differentiating Eq. (51) and using the definition of the kernel in Eq. (34). This gives:

$$EI(s)\theta'(s) = -F\int_0^s \theta(\xi)\,d\xi, \tag{52}$$

and, after differentiation:

$$\left(EI(s)\theta'(s)\right)' + F\theta(s) = 0. \tag{53}$$

Equation (52) directly yields the left-end condition $\theta'(0) = 0$. Moreover, evaluating Eq. (52) at $s = L$ and using the compatibility condition (50) gives $\theta'(L) = 0$. Hence, the linearized integral problem is equivalent to the Sturm–Liouville eigenvalue problem:

$$\begin{gathered}\left(EI(s)\theta'(s)\right)' + F\theta(s) = 0,\\ \theta'(0) = \theta'(L) = 0.\end{gathered} \tag{54}$$

For a homogeneous beam, $EI(s) = EI_0$, Eq. (54) reduces to:

$$\begin{gathered}\theta''(s) + \frac{F}{EI_0}\theta(s) = 0,\\ \theta'(0) = \theta'(L) = 0.\end{gathered} \tag{55}$$

The first non-trivial eigenvalue is therefore:

$$F_{cr} = \frac{\pi^2 EI_0}{L^2}. \tag{56}$$

Introducing the dimensionless load parameter:

$$\lambda = \frac{FL^2}{EI_0}, \tag{57}$$

one obtains:

$$\lambda_{cr} = \pi^2 \tag{58}$$

which is the classical Euler buckling load for a homogeneous pinned–pinned beam. The relation between the linearized problem and the nonlinear operator can also be stated directly in terms of its Fréchet derivative. Since $X_a$ is an affine subset rather than a vector space, the derivative is defined with respect to the associated perturbation space $X_0 = \{h \in C([0,L];\mathbb{R}) : h(0) = 0\}$. For the nonlinear operator $T_{a,F}$ defined by Eq. (45), the Fréchet derivative at $\theta \in X_a$ in the direction $h \in X_0$ is given by:

$$\left(DT_{a,F}[\theta]h\right)(s) = -F\int_0^s K(s,\xi)\cos\theta(\xi)\,h(\xi)\,d\xi. \tag{59}$$

At the trivial state $a = 0,\ \theta \equiv 0$, this becomes:

$$\left(DT_{a,F}[0]h\right)(s)=-F\int_0^s K(s,\xi)h(\xi)\,d\xi. \tag{60}$$

Thus, Eq. (51) can be written as:

$$\theta=DT_{0,F}[0]\theta, \tag{61}$$

showing that the linear eigenvalue problem governing the onset of buckling is precisely the linearization of the nonlinear integral formulation about the trivial equilibrium state. At the critical eigenvalues, the linearized problem admits non-trivial solutions, identifying the points at which non-trivial equilibrium branches may bifurcate from the trivial branch. The nonlinear integral equation then governs the corresponding finite-amplitude equilibrium states beyond the linearized bifurcation point.

### 4.5. Beam with constant bending stiffness

A particular case of the proposed model is a beam with constant bending stiffness:

$$EI(s)=EI_0=\text{const}. \tag{62}$$

In this case, the integral kernel defined by Eq. (34) simplifies to:

$$K(s,\xi)=\int_\xi^s\frac{d\eta}{EI_0}=\frac{s-\xi}{EI_0}. \tag{63}$$

Substituting Eq. (63) into Eq. (35) gives:

$$\theta(s)=a-\frac{F}{EI_0}\int_0^s(s-\xi)\sin\theta(\xi)\,d\xi. \tag{64}$$

The resulting equation is a nonlinear integral equation describing the finite-deflection equilibrium of a homogeneous Euler–Bernoulli beam. In this case, the influence of the mechanical properties of the member is reduced to the constant coefficient $EI_0$, whereas the entire integral kernel takes the simple form of a linear function of the distance between the points $s$ and $\xi$.

For the homogeneous beam, an exact nonlinear elastica solution is also available. For the first symmetric deflection branch, the relation between the prescribed end rotation $\theta_0$ and the dimensionless equilibrium load $\lambda$ defined by Eq. (57) is given by:

$$\lambda=4K^2\sin\left(\theta_0/2\right). \tag{65}$$

where $K(\cdot)$ denotes the complete elliptic integral of the first kind. This exact relation provides an analytical benchmark for the numerical solution of the nonlinear integral equation. Its quantitative comparison with the numerical results is presented in Section 5. The homogeneous case therefore provides a natural reference for more complex models with variable bending stiffness. Introducing the function $EI(s)$ replaces the simple kernel $(s-\xi)/EI_0$ with the more general function $K(s,\xi)$, while leaving the structure of the integral operator unchanged. Thus, the proposed integral equation constitutes a direct generalization of the classical homogeneous-beam model to the case of an arbitrarily varying bending-stiffness distribution.

### 4.6. Analytical properties of the nonlinear operator

The estimates established above allow several analytical properties of the nonlinear operator $T_{a,F}$ to be stated explicitly. First, using the inequality:

$$\left|\sin u-\sin v\right|\le\left|u-v\right|, \tag{66}$$

together with the kernel bound established in Section 4.1, for any $\theta_1$, $\theta_2\in X_a$ one obtains:

$$\left\|T_{a,F}\theta_1-T_{a,F}\theta_2\right\|_\infty\le F\max_{s\in[0,L]}\int_0^s K(s,\xi)\left|\theta_1(\xi)-\theta_2(\xi)\right|d\xi\le\frac{FL^2}{EI_{\min}}\left\|\theta_1-\theta_2\right\|_\infty. \tag{67}$$

Thus, $T_{a,F}$ is globally Lipschitz continuous on $X_a$, with Lipschitz constant not exceeding $FL^2/EI_{\min}$. In particular, if,

$$FL^2/EI_{\min}<1 \tag{68}$$

then $T_{a,F}$ is a contraction. Hence, by the Banach fixed-point theorem, for prescribed $a$ and $F$, the fixed-point equation $\theta=T_{a,F}\theta$ has a unique solution in $X_a$.

The operator $T_{a,F}$ is also compact. Let $B\subset X_a$ be bounded. Since $\left|\sin\theta\right|\le1$ and the kernel is uniformly bounded on the triangular domain, the family $T_{a,F}(B)$ is uniformly bounded. Moreover, the continuity of $K(s,\xi)$ on the compact triangular domain implies its uniform continuity. Consequently, $T_{a,F}(B)$ is equicontinuous. By the Arzelà–Ascoli theorem, $T_{a,F}(B)$ is relatively compact in $C([0,L])$. Therefore, $T_{a,F}$ is a compact operator.

As shown in Section 4.4, the operator $T_{a,F}$ is Fréchet differentiable with respect to $\theta$ and its derivative is given by Eq. (59). At the trivial equilibrium state $a=0$, $\theta\equiv0$, the derivative reduces to Eq. (60), which coincides with the linearized operator governing the onset of buckling.

The contraction condition (68) is a sufficient, but not necessary, condition for uniqueness of the fixed point for prescribed $a$ and $F$. It does not imply global uniqueness of the complete nonlinear equilibrium problem, in which the load $F$ is determined together with the rotation field $\theta$ through the scalar compatibility condition. In particular, global uniqueness should not be expected in the vicinity of a buckling bifurcation, where distinct equilibrium branches may coexist.

## 5. Numerical Example

To illustrate the application of the derived nonlinear integral equation, a simply supported beam with a locally reduced bending stiffness is considered. The stiffness distribution is assumed in the form:

$$EI(s) = EI_0\left(1 - \alpha \exp\left(-\left(\frac{s - s_0}{b}\right)^2\right)\right), \tag{69}$$

where $EI_0$ denotes the reference bending stiffness, $\alpha \in (0,1)$ defines the relative depth of the local reduction, $s_0$ specifies the location of its centre, and the parameter $b$ describes the extent of the stiffness variation. The adopted function makes it possible to model a smoothly varying local degradation without introducing discontinuities in the mechanical parameters.

Introducing the dimensionless coordinate:

$$z = s / L, \tag{70}$$

where $z \in [0,1]$, the bending-stiffness distribution can be written as:

$$EI(z) = EI_0 \rho(z), \tag{71}$$

where,

$$\rho(z) = 1 - \alpha \exp\left(-\left(\frac{z - z_0}{\beta}\right)^2\right) \tag{72}$$

and,

$$z_0 = s_0 / L, \quad \beta = b / L. \tag{73}$$

The function $\rho(z)$ describes the relative distribution of the bending stiffness. Introducing the dimensionless load parameter:

$$\lambda = \frac{FL^2}{EI_0} \tag{74}$$

and the dimensionless kernel:

$$\tilde{K}(z,\zeta) = \int_{\zeta}^{z} \frac{d\tau}{\rho(\tau)}, \tag{75}$$

the nonlinear integral equation (35) takes the dimensionless form:

$$\theta(z) = \theta(0) - \lambda \int_{\zeta}^{z} \tilde{K}(z,\zeta) \sin\theta(\zeta)\, d\zeta. \tag{76}$$

Equation (76) must be supplemented by the dimensionless compatibility condition

$$\int_0^1 \sin\theta(\zeta)\, d\zeta = 0. \tag{77}$$

For a prescribed stiffness distribution $\rho(z)$, the dimensionless kernel $\tilde{K}(z,\zeta)$ is evaluated numerically. Since it depends only on the prescribed stiffness distribution, it can be computed once and subsequently used throughout the solution procedure.

In the numerical example, a symmetrically located local stiffness reduction is adopted, with the parameters:

$$\alpha = 0.40, \quad \beta = 0.12, \quad z_0 = 0.50, \tag{78}$$

which means that the minimum bending stiffness at the midspan section is:

$$EI_{\min} = 0.60 EI_0. \tag{79}$$

To characterize the finite-amplitude equilibrium response, let $\theta_0 = \theta(0)$ denote the prescribed end rotation. For each prescribed value of $\theta_0$, the nonlinear integral equation together with the compatibility condition determines the corresponding equilibrium load parameter $\lambda$. The resulting solutions therefore define an equilibrium branch:

$$\lambda = \lambda(\theta_0). \tag{80}$$

The critical bifurcation load is obtained as the small-amplitude limit of this branch:

$$\lambda_{cr} = \lim_{\theta_0 \to 0} \lambda(\theta_0). \tag{81}$$

For the stiffness distribution defined by Eqs. (69)–(73), the equilibrium branch was evaluated for four prescribed rotation amplitudes. The obtained values are summarized in Table 1. The values approach:

$$\lambda_{cr} = 8.00636 \tag{82}$$

**Table 1.** Equilibrium load parameter for selected prescribed end rotations.

| $\theta_0$ [rad] | $\lambda(\theta_0)$ |
|---|---|
| 0.05 | 8.00616 |
| 0.10 | 8.01377 |
| 0.20 | 8.04430 |
| 0.40 | 8.16809 |

as $\theta_0 \to 0$. Thus, the previously reported value $\lambda = 8.04430$ for $\theta_0 = 0.20$ rad corresponds to a finite-amplitude equilibrium state rather than to the bifurcation load. It is approximately 0.51% higher than $\lambda_{cr}$.

The nonlinear integral equation (76) is discretized using the Nyström method [34, 35] with the trapezoidal quadrature rule. For each prescribed value of $\theta_0$, the discretized integral equation and the compatibility condition are solved simultaneously for the nodal values of the rotation field and the corresponding load parameter $\lambda$. A uniform discretization of the interval [0, 1] is introduced:

$$z_i = i / N, \quad i = 0,1,\ldots,N, \tag{83}$$

with the step size:

$$h = 1 / N. \tag{84}$$

For the integral appearing in Eq. (76), the composite trapezoidal rule gives:

$$\int_0^{z_i} K(z_i,\zeta) \sin\theta(\zeta) d\zeta \approx \sum_{j=0}^{i} w_{ij} \tilde{K}\left(z_i,z_j\right) \sin\theta_j \tag{85}$$

where $\theta_j = \theta(z_j)$ and the quadrature weights are:

$$w_{ij} = \begin{cases} h/2 & j=0 \text{ or } j=i, \\ h & 0<j<i. \end{cases} \tag{86}$$

Since $\tilde{K}(z_i,z_j) = 0$, the contribution associated with $j = i$ vanishes, but the standard trapezoidal form is retained for clarity. The discretized integral equation is therefore:

$$\theta_i = \theta_0 - \lambda \sum_{j=0}^{i} w_{ij} \tilde{K}\left(z_i,z_j\right) \sin\theta_j, \quad i = 1,\ldots,N. \tag{87}$$

The compatibility condition (77) is discretized using the same quadrature rule:

$$\sum_{j=0}^{N} w_j \sin\theta_j. \tag{88}$$

where,

$$w_j = \begin{cases} h/2 & j=0 \text{ or } j=i, \\ h & 0<j<N. \end{cases} \tag{89}$$

For a prescribed value of $\theta_0$, the unknown vector is:

$$u = \left(\theta_1, \theta_2, \ldots, \theta_N, \lambda\right)^T, \tag{90}$$

and therefore contains $N+1$ unknowns. The $N$ discretized integral equations (87), together with the compatibility condition (88), form a system of $N+1$ nonlinear algebraic equations.

The nonlinear algebraic system is written in residual form as:

$$\mathbf{R}(\mathbf{u}) = \mathbf{0}, \tag{91}$$

where,

$$R_i(\mathbf{u}) = \theta_i - \theta_0 + \lambda \sum_{j=0}^{i} w_{ij} \tilde{K}\left(z_i,z_j\right) \sin\theta_j, \quad i = 1,\ldots,N, \mathbb{F} \tag{92}$$

and the last component represents the compatibility condition:

$$R_{N+1}(\mathbf{u}) = \sum_{j=0}^{N} w_{ij} \sin\theta_j. \tag{93}$$

The nonlinear system is solved by Newton's method. At iteration $k$, the correction $\Delta u^{(k)}$ is determined from:

$$\mathbf{J}\left(\mathbf{u}^{(k)}\right) \Delta\mathbf{u}^{(k)} = -\mathbf{R}\left(\mathbf{u}^{(k)}\right). \tag{94}$$

where,

$$\mathbf{J}(\mathbf{u}) = \frac{\partial \mathbf{R}}{\partial \mathbf{u}}, \tag{95}$$

is the analytical Jacobian of the residual vector. The solution is then updated according to:

$$\mathbf{u}^{(k+1)} = \mathbf{u}^{(k)} + \Delta\mathbf{u}^{(k)}. \tag{96}$$

For $i, m = 1,\ldots,N$, the entries of the Jacobian associated with Eqs. (92) are:

$$\frac{\partial R_i}{\partial \theta_m} = \delta_{im} + \lambda w_{im} \tilde{K}(z_i,z_m) \cos\theta_m, \quad m \le i, \tag{97}$$

and,

$$\frac{\partial R_i}{\partial \theta_m} = 0, \quad m > i, \tag{98}$$

while differentiation with respect to the load parameter gives:

$$\frac{\partial R_i}{\partial \lambda} = \sum_{j=0}^{i} w_{ij} K(z_i, z_j) \sin\theta_j. \tag{99}$$

For the compatibility residual:

$$\frac{\partial R_{N+1}}{\partial \theta_m} = w_m \cos\theta_m, \quad m = 1, \dots, N, \tag{100}$$

and,

$$\frac{\partial R_{N+1}}{\partial \lambda} = 0. \tag{101}$$

The Newton iterations are initialized using the first symmetric buckling mode:

$$\theta^{(0)}(z) = \theta_0 \cos(\pi z), \tag{102}$$

together with the initial load estimate:

$$\lambda^{(0)} = 8.0. \tag{103}$$

The prescribed value $\theta_0$ is not included among the unknowns and remains fixed throughout the iterations. The Newton procedure is terminated when both:

$$\left\| \mathbf{R}\left(\mathbf{u}^{(k)}\right) \right\|_{\infty} < 10^{-10}, \tag{104}$$

and,

$$\left\| \Delta\left(\mathbf{u}^{(k)}\right) \right\|_{\infty} < 10^{-10}, \tag{105}$$

are satisfied.

Before examining the mesh convergence for the variable-stiffness beam, the accuracy of the numerical procedure was independently checked against the exact homogeneous-beam elastica solution given by Eq. (65). For the homogeneous case $\rho(z) = 1$ and the prescribed end rotation $\theta_0 = 0.20$ rad, the elliptic modulus appearing in Eq. (65) is $k = \sin(\theta_0 / 2) = \sin(0.10) = 0.09983341665$. The corresponding complete elliptic integral of the first kind is $K(k) = 1.57473234063$, and therefore Eq. (65) gives the exact finite-amplitude equilibrium load $\lambda_{exact} = 4K^2(k) = 9.91912777844$. The same homogeneous-beam problem was then solved using the Nyström discretization with the composite trapezoidal rule and $N = 400$. The numerical solution gives $\lambda_{\text{Nyström}} = 4K^2(k) = 9.91907679055$. The difference between the exact and numerical values is $\Delta\lambda = \lambda_{exact} - \lambda_{\text{Nyström}} = 5.09879 \cdot 10^{-5}$, which corresponds to the relative error $\varepsilon_{rel} = \Delta\lambda / \lambda_{exact} \times 100\% = 0.000514\%$. The close agreement with the exact elastica solution provides an independent quantitative verification of the Nyström implementation for the homogeneous-beam limit before applying the same numerical procedure to the beam with spatially variable bending stiffness.

To assess the numerical convergence of the Nyström discretization, calculations were performed for $N = 25, 50, 100, 200, 400$ for the prescribed amplitude $\theta_0 = 0.20$ rad. The corresponding load parameter, compatibility residual, and maximum residual of the discretized integral equations are listed in Table 2.

The results show systematic convergence of the load parameter with mesh refinement. The change in $\lambda$ between $N = 200$ and $N = 400$ is approximately $4.96 \cdot 10^{-5}$, corresponding to a relative difference of about $6.2 \cdot 10^{-6}$. Therefore, $N = 200$ provides sufficient accuracy for the subsequent calculations while retaining a moderate computational cost.

For all discretizations reported in Table 2, the nonlinear system converged in four Newton iterations from the initial estimate defined by Eqs. (102)–(103). The residual norms are close to machine precision and are therefore substantially smaller than the adopted stopping tolerance. For the reference discretization $N = 200$ and $\theta_0 = 0.20$ rad, the computed finite-amplitude equilibrium load is:

$$\lambda(0.20) = 8.044232. \tag{106}$$

This value is consistent with the value 8.04430 reported above for the equilibrium branch, the small difference being attributable to the numerical resolution used in the continuation calculation.

**Table 2.** Convergence of the Nyström discretization for $\theta_0$ = 0.20 rad.

| N | $\lambda$ | Compatibility residual | Maximum equation residual |
|---|---|---|---|
| 25 | 8.040055 | $8.67 \times 10^{-19}$ | $1.11 \times 10^{-16}$ |
| 50 | 8.043239 | 0.00 | $1.11 \times 10^{-16}$ |
| 100 | 8.044033 | $4.34 \times 10^{-19}$ | $1.11 \times 10^{-16}$ |
| 200 | 8.044232 | $1.39 \times 10^{-17}$ | $2.22 \times 10^{-16}$ |
| 400 | 8.044281 | 0.00 | $1.67 \times 10^{-16}$ |

As an independent verification, the corresponding differential boundary-value problem was also solved by a direct shooting method. Starting from the prescribed end rotation $\theta(0) = 0.20$ rad and the zero-moment condition $\theta'(0) = 0$, the load parameter was adjusted until the right-end condition $\theta'(1) = 0$ was satisfied. For the same stiffness distribution, the shooting solution gives:

$$\lambda_{shoot} = 8.044298. \tag{107}$$

This agrees closely with the Nyström result $\lambda = 8.044232$ obtained for $N = 200$. The relative difference between the two independent solutions is approximately $8.2 \cdot 10^{-6}$, providing an additional verification of the numerical integral-equation solution.

The physical deformed configuration of the beam is reconstructed from the computed rotation field. Introducing the dimensionless Cartesian coordinates:

$$\begin{aligned} \bar{x}(z) &= \int_0^z \cos\theta(\zeta)\, d\zeta, \\ \bar{y}(z) &= \int_0^z \sin\theta(\zeta)\, d\zeta. \end{aligned} \tag{108}$$

where $\bar{x} = x / L$, $\bar{y} = y / L$, the deformed centreline can be obtained directly from the numerical solution $\theta(z)$. For the representative case $\theta_0 = 0.20$ rad, the reconstructed configuration is presented together with the corresponding stiffness and rotation distributions in Fig. 2.

To illustrate the influence of the stiffness-distribution parameters on the finite-amplitude equilibrium load, a compact parametric study was performed for the prescribed rotation $\theta_0 = 0.20$ rad. In each series, one parameter was varied while the remaining two were kept at their reference values $\alpha = 0.40$, $\beta = 0.12$, $z_0 = 0.50$.

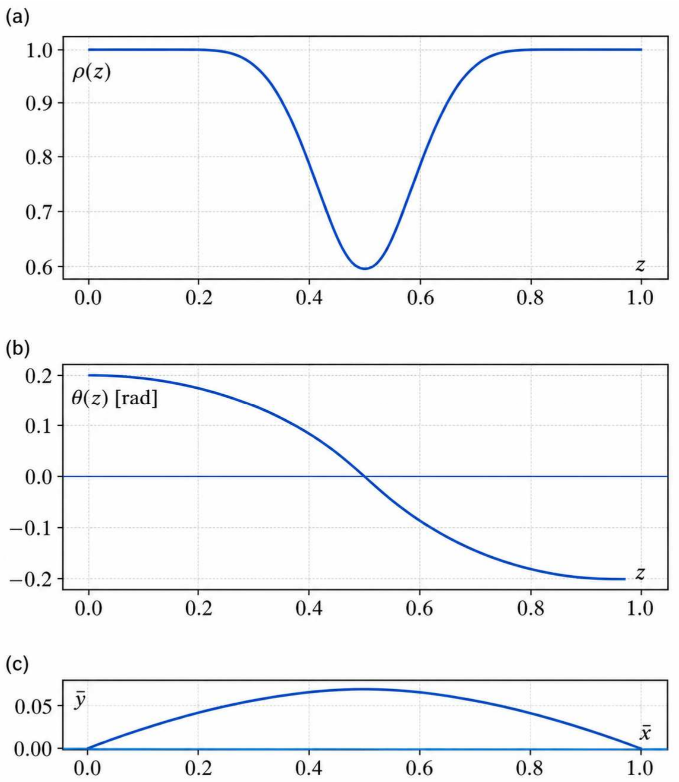


**Fig. 2.** (a) Relative bending-stiffness distribution $\rho(z)$, (b) corresponding rotation-angle distribution $\theta(z)$, (c) reconstructed dimensionless deformed centreline $\bar{y}(\bar{x})$ for $\theta_0 = 0.20$ rad.

**Table 3.** Influence of the stiffness-reduction parameters on the finite-amplitude equilibrium load.

| Varied parameter | Value | $\lambda$ ($\theta_0 = 0.20$ rad) |
|---|---|---|
| $\alpha$ | 0.20 | 9.06632 |
| $\alpha$ | 0.40 | 8.04430 |
| $\alpha$ | 0.60 | 6.75135 |
| $\beta$ | 0.08 | 8.54792 |
| $\beta$ | 0.12 | 8.04430 |
| $\beta$ | 0.16 | 7.64594 |
| $z_0$ | 0.25 | 8.78002 |
| $z_0$ | 0.50 | 8.04430 |
| $z_0$ | 0.75 | 8.79418 |

The results show that increasing either the degradation depth $\alpha$ or its spatial extent $\beta$ decreases the finite-amplitude equilibrium load. The location of the stiffness reduction also has a pronounced influence: for the present first symmetric equilibrium branch, a centrally located reduction produces a lower load than the corresponding off-centre cases. These results demonstrate that the effect of the variable bending stiffness is governed not only by the minimum stiffness value, but also by the spatial distribution incorporated into the kernel $\tilde{K}(z,\zeta)$.

From a broader perspective, the numerical results illustrate the principal advantage of the proposed integral formulation. In contrast to approaches based directly on the differential equilibrium equation, the spatial variation of the bending stiffness is represented entirely through the integral kernel, while the geometric nonlinearity retains the same functional form. Consequently, different stiffness distributions can be investigated without modifying the structure of the nonlinear operator. The agreement with the independent shooting solution confirms the mechanical equivalence of the integral and differential formulations, whereas the parametric results demonstrate that the kernel provides a direct representation of the influence of the spatial stiffness distribution on the finite-amplitude equilibrium response. The present formulation should therefore be regarded not as a replacement for established differential or finite-element approaches, but as a complementary representation that is particularly suitable for operator-theoretic analysis and integral-equation-based numerical methods.

## 6. Conclusions

This paper has presented an equivalent nonlinear Volterra integral formulation with Hammerstein-type nonlinearity for the finite-deflection equilibrium analysis of a planar, inextensible Euler–Bernoulli beam with variable bending stiffness subjected to a conservative compressive dead load. Once the governing inextensible elastica model is adopted, the transformation from the differential equation to the integral formulation introduces no further approximation and preserves the equivalence with the original boundary-value problem when supplemented by the scalar compatibility condition.

The resulting formulation separates the spatial variation of the bending stiffness, represented by the integral kernel, from the geometric nonlinearity associated with the rotation field. The analytical properties established for the nonlinear operator include a uniform kernel bound, global Lipschitz continuity, a sufficient contraction condition for uniqueness at prescribed parameters, compactness, and Fréchet differentiability. Linearization about the trivial equilibrium state leads directly to the corresponding Sturm–Liouville eigenvalue problem and recovers the classical Euler critical load for a homogeneous pinned–pinned beam. The homogeneous nonlinear elastica solution also provides an exact benchmark for the finite-amplitude formulation.

The numerical results demonstrate the distinction between the critical bifurcation load and the finite-amplitude equilibrium load. The Nyström discretization shows systematic convergence and agrees closely with an independent shooting solution of the differential boundary-value problem. The reconstructed deformed centreline and the parametric study further show how the depth, width, and location of a local stiffness reduction affect the finite-amplitude equilibrium response.

The proposed integral representation therefore provides a consistent framework for analytical and numerical investigations of finite-deflection equilibrium and stability-related problems of beams with spatially variable bending stiffness. Further work may address broader existence results for the augmented nonlinear problem, continuation and bifurcation analysis, alternative numerical schemes for the integral formulation, and extensions to more general structural models.

## Author Contributions

M. Sadowski conceived the study, developed the mathematical formulation, performed the theoretical analysis, carried out the numerical computations, interpreted the results, and wrote the manuscript.


## Acknowledgments

Not applicable.


## Conflict of Interest

The author declares no conflict of interest.


## Funding

This research received no external funding.


## Data Availability Statements

The numerical data supporting the findings of this study, including the nodal solution, stiffness-kernel values, solver settings, and convergence data, are provided in the Supplementary Material.

## Nomenclature

**Dimensional variables**

| | |
|---|---|
| $F$ | Compressive force |
| $EI(s)$ | Spatially varying bending stiffness |
| $EI_0$ | Reference bending stiffness |
| $EI_{min}$ | Minimum bending stiffness |
| $L$ | Undeformed beam length |
| $s$ | Material arc-length coordinate |
| $x(s), y(s)$ | Cartesian coordinates of the deformed beam centreline |
| $w(x)$ | Transverse displacement of the beam axis |
| $M(s)$ | Bending moment |
| $\kappa(s)$ | Curvature of the deformed beam centreline |
| $\theta(s)$ | Rotation angle of the beam centreline |
| $a$ | Prescribed initial rotation, $a = \theta(0)$ |
| $u(s)$ | Transformed rotation variable, $u = \tan(\theta / 2)$ |
| $K(s,\xi)$ | Integral kernel associated with the bending-stiffness distribution |
| $s$ | Location of the centre of the local stiffness reduction |
| $b$ | Parameter describing the spatial extent of the local stiffness reduction |
| $\xi,\eta$ | Integration variables |

**Dimensionless variables and parameters**

| | |
|---|---|
| $z$ | Dimensionless arc-length coordinate |
| $z_0$ | Dimensionless location of the centre of the stiffness reduction |
| $\beta$ | Dimensionless width parameter of the stiffness reduction |
| $\alpha$ | Relative depth of the local stiffness reduction |
| $\rho(z)$ | Relative bending-stiffness distribution |
| $\lambda$ | Dimensionless compressive load parameter |
| $\lambda_{cr}$ | Dimensionless critical bifurcation load |
| $\tilde{K}(z,\zeta)$ | Dimensionless integral kernel |
| $\theta$ | Prescribed end rotation used to parameterize the equilibrium branch |
| $\zeta,\eta$ | Dimensionless integration variables |
| $\overline{x},\overline{y}$ | Dimensionless Cartesian coordinates of the deformed centreline |

**Operators and functionals**

| | |
|---|---|
| $X_a$ | Affine subset of $C([0,L];\mathbb{R})$ satisfying $\theta(0)=a$ |
| $T_{(a.F)}$ | Nonlinear Volterra integral operator |
| $C_F[\theta]$ | Scalar compatibility functional associated with the right-end moment condition |
| $f(s)$ | Linear part of the general Volterra–Hammerstein equation |
| $g(\xi,\theta)$ | Nonlinear function in the integral equation |
| $D_\theta T_{(a.F)}$ | Fréchet derivative of the nonlinear operator with respect to $\theta$ |
| $\Vert\cdot\Vert_\infty$ | Supremum norm |

**Numerical quantities**

| | |
|---|---|
| $N$ | Number of subintervals in the Nyström discretization |
| $h$ | Dimensionless discretization step |
| $z_i$ | Discretization nodes |
| $\theta$ | Nodal values of the rotation field |
| $w_i^{(i)}$ | Trapezoidal quadrature weights |
| $\mathbf{q}$ | Vector of unknown nodal rotations and load parameter |
| $\mathbf{R}(\mathbf{q})$ | Nonlinear residual vector |
| $R_i$ | Residual of the $i$-th discretized integral equation |
| $R$ | Compatibility residual |
| $\mathbf{J}(\mathbf{q})$ | Analytical Jacobian matrix |
| $\Delta\mathbf{q}$ | Newton correction vector |
| $k$ | Newton iteration index |

## References


[1] Sadowski, M., *Spatial Shaping of Compressed Rods with Maximum Buckling Load Capacity*, Ph. D. Thesis, University of Zielona Góra, Zielona Góra, Poland, 2018.
[2] Marcinowski, J., *Nonlinear Stability of Elastic Shells*, Publishing House of Wrocław University of Science and Technology, Wrocław, Poland, 1999.
[3] Bazant, Z.P., Cedolin, L., *Stability of Structures: Elastic, Inelastic, Fracture and Damage Theories*, Oxford University Press, New York, 1991.
[4] Jerath, S., *Structural Stability Theory and Practice: Buckling of Columns, Beams, Plates, and Shells*, Wiley, 2021.
[5] Euler, L., *Methodus inveniendi lineas curvas maximi minimive proprietate gaudentes, sive solutio problematis isoperimetrici latissimo sensu accepti. Additamentum I De curvis elasticis*, Apud Marcum-Michaelem Bousquet et Socios, Lausanne and Geneva, 1744.
[6] Timoshenko, S.P., Gere, J.M., *Theory of Elastic Stability*, 2nd ed., McGraw-Hill, New York, 1961.
[7] Koiter, W.T., *On the Stability of Elastic Equilibrium*, Ph. D. Thesis, Delft University of Technology, Delft, 1945.
[8] Bendsøe, M.P., Sigmund, O., *Topology Optimization: Theory, Methods and Applications*, Springer, 2003.
[9] Lee, B.K., Wilson, J.F., Oh, S.J., Elastica of Cantilevered Beams with Variable Cross Sections, *International Journal of Non-Linear Mechanics*, 28, 1993, 579–589. DOI: 10.1016/0020-7462(93)90049-Q.
[10] Darbandi, S.M., Firouz-Abadi, R.D., Haddadpour, H., Buckling of Variable Section Columns under Axial Loading, *Journal of Engineering Mechanics*, 136, 2010, 472–476.
[11] Gross, O., Pinkall, U., Wahl, M., Elastic Curves with Variable Bending Stiffness, *Studies in Applied Mathematics*, 155(2), 2025, e70097.
[12] Antman, S.S., *Nonlinear Problems of Elasticity*, 2nd ed., Springer, New York, 2005.
[13] Sadowski, M., Analytical classification of buckling problems of compressed rods with variable bending stiffness using special functions, *Civil and Environmental Engineering Reports*, 36(2), 2026, 133–149.
[14] Huang, Y., Li, X.-F., Buckling Analysis of Nonuniform and Axially Graded Columns with Varying Flexural Rigidity, *Journal of Engineering Mechanics*, 137(1), 2011, 13–24.
[15] Wu, K., Zheng, G., Insight into numerical solutions of static large deflection of general planar beams for compliant mechanisms, *Mechanism and Machine Theory*, 172, 2022, 104757.
[16] Magnusson, A., Ristinmaa, M., Ljung, C., Behaviour of the Extensible Elastica Solution, *International Journal of Solids and Structures*, 38(46–47), 2001, 8441–8457.
[17] Ibrahimbegovic, A., Shakourzadeh, H., Batoz, J.-L., Al Mikdad, M., Guo, Y.-Q., On the Role of Geometrically Exact and Second-Order Theories in Buckling and Post-Buckling Analysis of Three-Dimensional Beam Structures, *Computers & Structures*, 61(6), 1996, 1101–1114.
[18] Farokhi, H., Ghayesh, M.H., A New Geometrically Exact Model for Buckling and Postbuckling Statics and Dynamics of Beams, *Journal of Applied Mechanics*, 86(7), 2019, 071001.
[19] Maassen, S., da Costa e Silva, C., de Mattos Pimenta, P., Schröder, J., On a Geometrically Exact Euler–Bernoulli Beam Element, *Proceedings in Applied Mathematics and Mechanics*, 18(1), 2018, e201800079.
[20] Hafeez, M.B., Krawczuk, M., A Review: Applications of the Spectral Finite Element Method, *Archives of Computational Methods in Engineering*, 30, 2023, 3453–3465.
[21] Elfelsoufi, Z., Azrar, L., Buckling, Flutter and Vibration Analyses of Beams by Integral Equation Formulations, *Computers & Structures*, 83(31–32), 2005, 2632–2649.
[22] Krasnosel'skii, M.A., Zabreiko, P.P., Pustyl'nik, E.I., Sobolevskii, P.E., *Integral Operators in Spaces of Summable Functions*, Noordhoff International Publishing, Leiden, 1976.
[23] Kress, R., *Linear Integral Equations*, 4th ed., Springer, Cham, 2023.
[24] Gripenberg, G., Londen, S.-O., Staffans, O., *Volterra Integral and Functional Equations*, Encyclopedia of Mathematics and Its Applications, Vol. 34, Cambridge University Press, Cambridge, 1990.
[25] Brunner, H., *Collocation Methods for Volterra Integral and Related Functional Differential Equations*, Cambridge Monographs on Applied and Computational Mathematics, Vol. 15, Cambridge University Press, Cambridge, 2004. ISBN 978-0-521-80615-2.
[26] Gere, J.M., Goodno, B.J., *Mechanics of Materials*, 9th ed., Cengage Learning, 2018.
[27] Sadd, M.H., *Elasticity: Theory, Applications, and Numerics*, 4th ed., Academic Press, 2020.
[28] Wang, C.M., Reddy, J.N., Lee, K.H., *Shear Deformable Beams and Plates*, Elsevier, 2000.

[29] Audoly, B., Pomeau, Y., *Elasticity and Geometry: From Hair Curls to the Nonlinear Response of Shells*, Oxford University Press, 2010.
[30] Carmo do, M.P., *Differential Geometry of Curves and Surfaces*, Prentice-Hall, 1976.
[31] Borkovic, A., Marussig, B., Radenkovic, G., Geometrically Exact Static Isogeometric Analysis of an Arbitrarily Curved Spatial Bernoulli–Euler Beam, *Computer Methods in Applied Mechanics and Engineering*, 390, 2022, 114447.
[32] Piskorek, A., *Integral Equations*, WNT – Scientific and Technical Publishers, Warsaw, Poland, 1983.
[33] Pietrowski, I., *Lectures on Integral Equations*, translated by S. Drobot, Polish Mathematical Society, Warsaw–Wrocław, Poland, 1951.
[34] Atkinson, K.E., *The Numerical Solution of Integral Equations of the Second Kind*, Cambridge University Press, Cambridge, 1997.
[35] Barrera, D., Bartoni, M., Chiarella, I., Remogna, S., On numerical solution of Fredholm and Hammerstein integral equations via Nyström method and Gaussian quadrature rules for splines, *Applied Numerical Mathematics*, 174, 2022, 71–88.

## ORCID iD

Mirosław Sadowski https://orcid.org/0009-0007-7886-7666



**How to cite this article:** Sadowski M. A Nonlinear Integral Equation for Finite-Deflection Analysis of an Euler–Bernoulli Beam with Variable Bending Stiffness, *J. Appl. Comput. Mech.*, xx(x), 2026, 1–15. https://doi.org/10.22055/jacm.2026.49578.6088